water

MDPI

Article

Numerical Simulations of Non-Point Source Pollution in a Small Urban Catchment: Identification of Pollution Risk Areas and Effectiveness of Source-Control Measures

Ye Pan, Jiaxun Guo, Long Yang, Qiqi Yuan, Zhihui Ren and Lachun Wang *

School of Geography and Ocean Science, Nanjing University, Nanjing 210023, China; dg1927025@smail.nju.edu.cn (Y.P.); dg1727009@smail.nju.edu.cn (J.G.); yanglong@nju.edu.cn (L.Y.); DZ1827004@smail.nju.edu.cn (Q.Y.); mg1827016@smail.nju.edu.cn (Z.R.)
* Correspondence: wang6312@nju.edu.cn; Tel.: +86-025-8359-3233

Abstract: Urban non-point source pollution is becoming a serious issue under the context of rapid urbanization and its impacts on surface hydrologic processes. The identification of non-point source risk areas and the effectiveness of source-control measures provides important first steps to improve the degrading aquatic environment but is challenged by the complex dynamics and variabilities of surface pollutants in urban environments. In this study, we investigate the spatial and temporal variabilities of non-point source pollution in a small urban catchment based on numerical simulations and in-situ samplings. Our results show that residential, industrial, and commercial land contribute to the most pollutant loadings and are the main constituents of the pollution risk area. Rainfall duration and intensity are the main factors in determining the temporal variations of urban non-point source pollution. There is no correlation between early drought days and pollution load. Numerical simulations show that it is more effective to increase urban vegetation coverage than to enhance road cleaning for effective non-surface pollution control. For enhanced road cleaning, it is more effective to improve the frequency of road cleaning than its efficiency. Our results provide important guidance for effective controls of non-point source pollution as well as the establishment of long-term surface pollutant monitoring network in complex urban environments.

Keywords: urban non-point source pollution; SWMM; urban hydrology; source control measures

Citation: Pan, Y.; Guo, J.; Yang, L.; Yuan, Q.; Ren, Z.; Wang, L. Numerical Simulations of Non-Point Source Pollution in a Small Urban Catchment: Identification of Pollution Risk Areas and Effectiveness of Source-Control Measures. *Water* **2021**, *13*, 96. https://doi.org/10.3390/w13010096

Received: 17 November 2020
Accepted: 30 December 2020
Published: 4 January 2021

1. Introduction

Rapid urbanization leads to expansion of impervious coverages, and poses strong alternations to surface hydrologic processes [1]. These alternations further induce degradations of aquatic environment in urban channels and adjacent water bodies through point-source pollution (i.e., sewage pipes [2]) and non-point source pollution (i.e., storm runoff [3]). While the point-source pollution has been effectively controlled in most regions, the non-point source pollution in complex urban environments becomes an increasingly important concern [4]. Statistics show that urban non-point source pollution has become the second largest non-point source pollution [5].

Urban non-point source pollution refers to the processes of water pollution where dissolved or solid pollutants accumulated on days without rain, and are carried by surface runoff into the receiving waters through surface storm runoff or pipe flows during rainy days [6]. There are several sources that contribute to urban non-point pollution, including atmospheric deposition, vehicular transportation-related activities, and metallic building envelopes. For instance, Hou et al. [7] found that atmospheric deposition predominantly contributes to roof runoff pollution in Beijing. Pitt et al. [8] concluded that vehicle service areas, and parking and storage facilities contribute both conventional pollutants and micropollutants to stormwater runoff in industrial and commercial areas. Residential areas, parks, and lawns are generally areas with high pedestrian traffic, and thus may be the main

sources of fecal bacteria, nutrients, and solids to urban runoff [9]. Rainwater corrosion on the exterior of buildings is also the sources of rainfall runoff pollution. For example, buildings were found to be a dominant source of alkylphenols in field measurements of atmospheric deposition and stormwater runoff in a suburban catchment near Paris [10]. The main pollutants from these sources are total nitrogen (TN), total phosphorus (TP), chemical oxygen demand (COD), total suspended solid (TSS), alkylphenols (APs), and so on [11]. The production and transport of these potential source pollution eventually affect the water quality of the receiving water bodies, causing a series of environmental problems, such as eutrophication [12]. The eutrophication of water bodies is mainly caused by excessive input of nitrogen and phosphorus, which subsequently threatens natural ecosystems and drinking water safety [13]. For example, the appalling drinking water crisis occurred in Wuxi City in 2007 due to contaminations of cyanobacterial blooms in Taihu Lake [14].

The urban non-point source pollution is heterogeneously distributed in both space and time, which is mainly due to its random characteristics, complex influencing factors, and different pollutant types [15]. From the spatial perspective, urban non-point source pollution is mainly associated with surface imperviousness [16], land use type [17,18], and drainage network structure [19]. For instance, Cheng et al. [20] found that in areas with non-point source pollution load in watershed with high forest coverage is smaller than other areas. From the temporal perspective, the pollution load is related to different rainfall characteristics, such as storm total rainfall, rainfall duration, rainfall intensity [21], and early drought days (i.e., number of days without rain [22]). Previous studies show that larger rainfall intensities and storm total rainfall amount lead to stronger scouring, leaching, dilution, and dissolution effects of rainwater on surface pollutants [21]. Longer early drought days, which tend to accumulate more surface pollutants, lead to higher potentials of non-point source pollution in urban environments [22]. Previous studies investigated the properties of urban non-point source pollution based on in-situ monitoring and numerical simulations [23]. Among them, particular attention of in-situ monitoring has been given to the initial flushing effect of pollution [24,25]. In-site monitoring has advantages in providing direct evidence of non-point source pollution in urban environments. However, in-site monitoring usually adopts event-average concentration to estimate non-point source pollution load [19,20], it is thus difficult to accurately estimate the non-point source pollution load at the scale of small urban catchments (i.e., less than 50 km^2) with heterogeneities in land surface properties.

In order to fully understand and deal with the issue of urban non-point source pollution, a number of numerical models have been developed to simulate the dynamics of surface pollutant, such as Hydrological Simulation Program-Fortran (HSPF) [26], Storm Water Management Model (SWMM) [27], the Storage, Treatment, and Overflow, Runoff Model (Storm) [28], Distributed Routing Rainfall-Runoff Model (DR3M-QUAL) [29], etc. With the aid of distributed processes simulated by numerical models, the spatial and temporal characteristics of urban non-point source pollution can be analyzed [30,31]. It is of great help to calculate the current situation of urban non-point source pollution, and provide suggestions for the control of urban non-point source pollution [32–35]. As a semi-distributed continuous simulation model, SWMM has shown great advantages in simulating storm runoff response and non-point source pollution in urban areas [36,37]. It is thus mostly recommended for research and practical management of urban non-point source pollution [38–41]. Most studies on urban non-point source pollution using SWMM focus on the control research and treatment hypothesis of non-point source pollution by following the principle of best management practices (BMPs) [32]. However, few studies have been carried out to identify non-point source pollution risk areas in highly urbanized areas based on SWMM.

Non-point source pollution risk area threatens the water safety seriously. Controlling the key non-point source pollution risk area can control non-point source pollution to the greatest extent at the minimum cost [42]. Hence, when the backend problem of non-

point source pollution cannot be effectively solved, source control by analyzing the risk probability is becoming important [43]. In addition, source-control of non-point source pollution is one part of the pollution control system (including sink control and end control). Source control measures refer to a series of measures taken against non-point source pollution before a large amount of runoff is generated, such as green roof, permeable pavement, etc. [44]. Increasing the surface vegetation coverage can effectively reduce storm runoff and increase the absorption and filtration loadings of pollutants by vegetation and soil, leading to the reduction of non-point source pollutants. Previous studies show that increasing the frequency and efficiency of road cleaning can effectively reduce the cumulative load of surface non-point source pollution [45]. The purpose of this study is thus to provide useful references for the identification and control of urban non-point source pollution in a small urban catchment based on in-situ samplings and SWMM simulations.

The rest of the paper is organized as follows. In Section 2, we briefly describe the location of study area and in-situ samplings. We set up the SWMM model in our study region in Section 3. We show the spatial and temporal variations of TN and TP loadings from SWMM simulations in Section 4. The effectiveness of different source-control measures is also evaluated in Section 4, followed by summary and conclusions in Section 5.

2. Study Area and In-Situ Observations

2.1. Study Area

Our study area is located in a small urban catchment in Wuxi, Jiangsu province, China (see Figure 1 for its location). The city of Wuxi is a typical lakeside city adjacent to the Taihu Lake, the third largest freshwater lake in China. The water pollution of Taihu Lake has been the focus of public attention [46]. Fast urbanization around the lake has taken place in recent decades, and pose challenges to water quality in the lake [12,47]. Our study area lies in a subtropical monsoon climate, with rainfall accumulated during April to September accounting for 70% of the average annual total rainfall of 1115.5 mm [48]. Our study catchment is a hydrologically closed catchment, with its boundaries distinct by either a canal/urban channel or the lake (Figure 1). The total drainage area of the catchment is 36 km^2. The study area is characterized by complicated river networks (i.e., 29 urban channels in total) over relatively flat terrains. These urban channels are hydrologically disconnected from each other through regulation by weirs and sluices, leading to extremely stagnant flows. The storm drainage system is separated, with domestic sewage diverted into a sewage treatment plant, while storm runoff drains into the channels directly.

Figure 1. Location of study area and four sampling sites. I–IV indicates the four sub-catchments that dominated by residence, park, commercial area, and greenbelt, respectively.

Figure 2 provides an overview of elevation, land use/land cover, and layouts of the storm drainage system within the catchment. The elevation data are provided by Google maps with a spatial resolution of 33 m. The land use/land cover is derived from visual inspections of remote sensing images provided by Google earth with a spatial resolution of 0.25 m. The impervious area accounts for 58.8% of the entire drainage area. There are 11 land use/land cover types within the study area (Figure 2b). They are residential land (41.2%), cultivated land (16.3%), industrial land (12.9%), green spaces (10.1%), roads (9.5%), commercial land (3.5%), education land (mainly schools) (2.7%), water body (1.7%), public services land (mainly medical and health land, government agency land, and social welfare land) (1.3%), bare land (0.6%), and religious land (mainly temples and churches) (0.2%). Except for roads and water body, each land use/land cover type is composed of three land surface units, i.e., greenbelt, pavement, and roof. The areal proportion occupied by the three land surface units for each land use and land cover type is shown in Figure 3. The layouts of storm drainage system are provided by Nanjing Hydraulic Research Institute (Figure 2d).

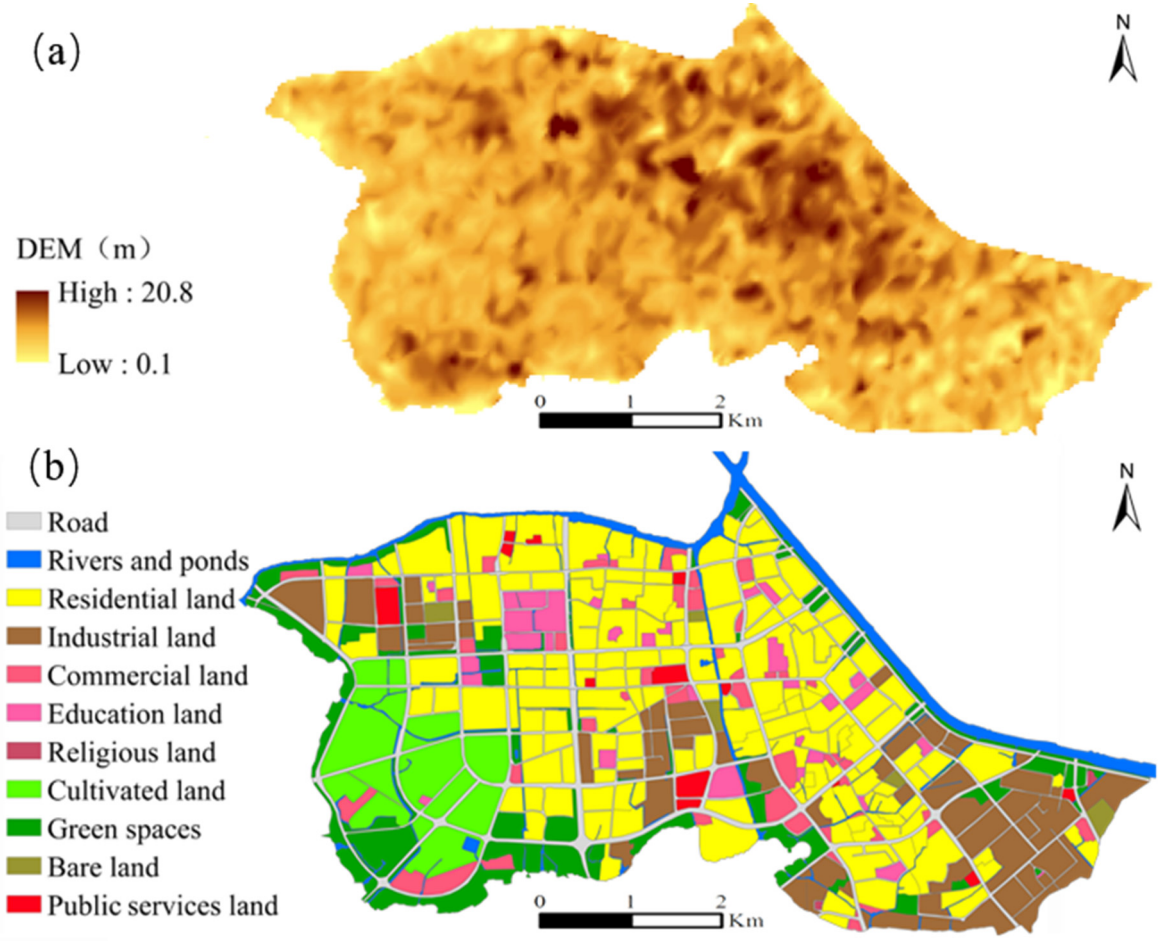

Figure 2. *Cont.*

Figure 2. Key static variables and frames for Storm Water Management Model (SWMM). (**a**) DEM; (**b**) land use type; (**c**) sub-catchment of study area; (**d**) drainage system generalization of study area.

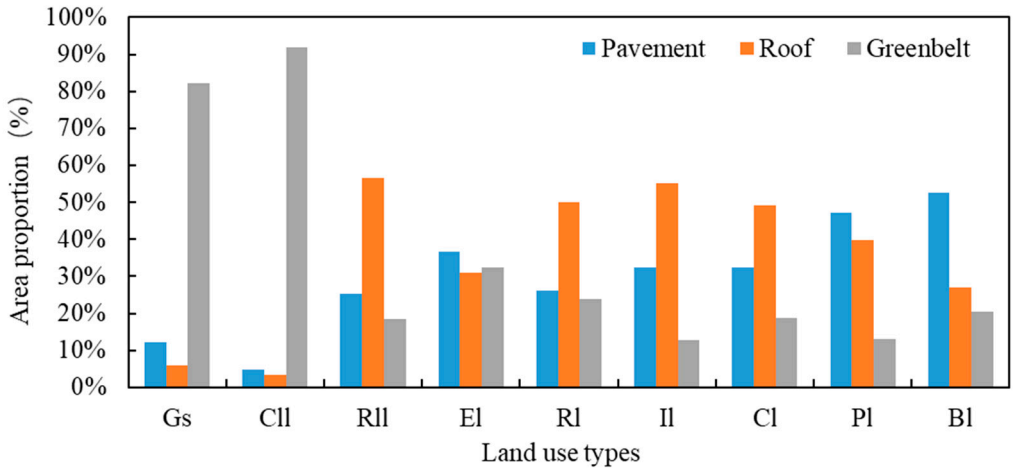

Figure 3. Area proportions of land surface areas of different land use types. The abbreviations on the x-axis are expanded as follows: Gs—Green spaces; Cll—Cultivated land; Rll—Religious land; El–Education land; Rl—Residential land; Il—Industrial land; Cl—Commercial land; Pl—Public services land; Bl—Bare land.

2.2. In-Situ Observations

There are two rain gauges in the vicinity of our study area, with observed hourly rainfall during the entire study period and one-minute rainfall observations collected during the study period 2018–2019 (see Figure 1 for their locations). In addition, stormwater

was collected to analyze the concentration of pollutants in rainfall. The rainfall observations are mainly used to provide meteorological forcing for numerical simulations.

In addition to rainfall observations, we collected surface storm runoff samples over four sub-catchments with contrasting land use/land cover types (see Figure 1 for their locations). These sub-catchments were selected based on their accessibility and the areal proportion of the three land surface units in each sub-catchment. The land use/land cover types of the four sub-catchments of I–IV are residential land, industrial land, commercial land, and green spaces, respectively. The storm total runoff was collected for two storm events, i.e., 19–20 June 2018 and 9 April 2019. The collected storm runoff samples were immediately stored in a portable refrigerator and transported to laboratory for analyses. The collected storm runoff samples were used for TN and TP analysis before filtration. The potassium persulfate oxidation-ultraviolet spectrophotometry was used for TN analysis. The potassium persulfate digestion-molybdenum-antimony anti-spectrophotometry was used for TP analysis. The monitoring limit of the method was 0.001 mg/L. The sample analyses were implemented by Nanjing Institute of Geography and Limnology, Chinese Academy of Sciences.

3. Model Setup

3.1. Model Configuration

The SWMM model is developed by United States Environmental Protection Agency (USEPA). It is a semi-distributed hydrological model for dynamic rainfall-runoff simulation [49]. We use version 5.1 of the SWMM model (USEPA, Cincinnati, OH, USA) in this study. We discretize the catchment into 515 sub-catchments, with an average area of 6.75 ha. There are 1282 rainwater pipe nodes, 1222 main rainwater pipelines, and 117 drainage outlets. The length of rainwater pipelines ranges from 3 m to 853 m. The SWMM model differentiates three land surface units (i.e., pavement, roof, and greenbelt) in each sub-catchment. Although in reality the greenbelt is a mixture of grasses and trees in our study area, the model assumes only grasses for the greenbelt. This might be a source of simulation uncertainty, but since the set-up of greenbelts is uniform across the study region in the real world, we believe our conclusions would still hold despite this simple treatment. Runoff generation and pollutant loading processes are simulated at the sub-catchment scale. The pollutant migration is simulated through the "pipe-node" simulation (see Rossman [50] for details).

The SWMM model adopts the nonlinear reservoir method to generalize runoff production and confluence processes. Channel streamflow is simulated based on the Saint Venant's equation and the Manning's equation [51]. We use the Horton model to calculate soil infiltration, due to the fact that the major portion of the catchment is impervious. The dynamic wave method is chosen for simulating flow in pipes. In terms of water quality simulation, we set the initial values of TN and TP. These initial values, that is, the generation of pollutants, come from our actual measurements of the pollutant concentration in multiple rainfall events [39]. We use the saturation function as the surface pollutant build-up algorithm in SWMM. The exponential function is used as the surface pollutant wash-off algorithm in this study. The variation of water quality in the conduit is assumed to follow a continuous stirred tank reactor [52].

Urban non-point source pollution mainly comes from atmospheric deposition, drainage surfaces, anthropogenic activities, and urban drainage systems [3]. For the generation and accumulation of surface pollutants, the SWMM model only considers the pollutant concentration in rainfall and the calculation process of pollutant build-up in the three land surface units. This might be a source of simulation uncertainty. However, either precipitation or deposition in dry weather can be assumed uniform in a small catchment [7]. Anthropogenic activities can occur in any place such as industrial and commercial areas, parks, residential areas, etc., and the surfaces of urban buildings are susceptible to rain erosion [8–10]. Therefore, we believe that the sources of urban non-point source pollution

are relatively evenly accumulated in space or accumulated in built-up areas more and these uncertainties are not important to our results.

The model simulations are implemented with a time interval of one hour, and are carried out for throughout 2018, i.e., from 1st January to 31st December.

3.2. Model Parameters

The parameters of SWMM include hydrologic parameters, hydraulic parameters, and water quality parameters. Based on the analysis of geographical data (i.e., digital elevation, land use/land cover), we determine the drainage area of each sub-catchment, overflow width of each sub-catchment, average surface slope, and percentage of impervious area. The geometrical parameters of storm pipes, including pipe diameter, conduit length, inlet offset of conduit, and outlet offset of conduit, were extracted from the metadata of storm drainage network provided by the Nanjing Hydraulic Research Institute.

The ranges of hydrologic and hydraulic parameters were determined by referring to the SWMM model manual and previous studies [50,53,54]. The ranges of the parameters are listed in Table 1. The dynamic processes of TN and TP loadings are first simulated over each of the three land units (i.e., pavement, roof, and greenbelt), and are then integrated as the main output from each sub-catchment. The valid ranges of relevant parameters over three land units are listed in Table 2.

Table 1. Major hydrological, hydraulic parameters of SWMM, and their value ranges.

Parameter	Meaning	Unit	Value Range
N-Imperv	Mannings N of impervious area	$s \cdot m^{-1/3}$	0.011–0.024
N-perv	Mannings N of pervious area	$s \cdot m^{-1/3}$	0.03–0.24
Dstore-Imperv	Depth of depression storage on impervious area	mm	1.27–2.54
Dstore-perv	Depth of depression storage on pervious area	mm	2.54–5.08
Zero-Imperv	Percent of impervious area with no depression storage	%	5–30
MinRate	Minimum rate on the Horton infiltration curve	mm/h	0.3–9.9
MaxRate	Maximum rate on the Horton infiltration curve	mm/h	25.4–91.44
Decay	Decay constant for the Horton infiltration curve	h^{-1}	2–6
Drying Time	Time for a fully saturated soil to completely dry	day	2–14
Manning-N	Manning's roughness coefficient of pipe	$s \cdot m^{-1/3}$	0.013–0.014

Table 2. Value ranges of water quality parameters on different land surface units in SWMM.

Area	Parameter	Unit	Value Range	
			TN	TP
Greenbelt	Maximum accumulation quantity	$kg \cdot ha^{-1}$	7.5–10	0.6–1.8
	Half-saturation constant	day	4–10	8–10
	Wash off coefficient	mm^{-1}	0.002–0.005	0.001–0.004
	Wash off exponent	-	1.1–1.4	1.2–1.3
Pavement	Maximum accumulation quantity	$kg \cdot ha^{-1}$	3.8–6	0.2–0.6
	Half-saturation constant	d	4–11	10–11
	Wash off coefficient	mm^{-1}	0.004–0.009	0.001–0.008
	Wash off exponent	-	1.1–1.8	1.25–1.9
	Removal rate by street sweeping	%	50–75	50–75
Roof	Maximum accumulation quantity	$kg \cdot ha^{-1}$	2.2–4	0.2–0.6
	Half-saturation constant	d	4–10	8–10
	Wash off coefficient	mm^{-1}	0.004–0.007	0.001–0.006
	Wash off exponent	-	1.3–1.9	1.25–1.9

We carried out a sensitivity analysis for the parameters listed in Tables 1 and 2 to obtain a better understanding of how the simulated results are sensitive to model parameters. The sensitivity analysis is based on the modified Morris screening method in the local sensitivity analysis [55]. The basic idea of the method is to change the value of each parameter by a certain percentage for each simulation, and compare simulation results (i.e., runoff, peak

discharge, TN, and TP loadings) with the default results where no changes are made. The change rate 5% is typically used for sensitivity analysis [55]. Three rainfall events, i.e., 22–23 July 2018, 29 July 2018, and 21 August 2018, were selected for sensitivity analysis. The three events are contrasted with rainfall intensities, durations, and antecedent conditions. Table 3 shows the top four most sensitive parameters (with 1 being most sensitive) for the simulations of runoff, peak discharge, TN, and TP loadings, respectively. These parameters are particularly focused on during the model calibration processes.

Table 3. Sensitivity ranking of parameters in SWMM.

Ranking \ Outputs	Runoff	Peak Discharge	TN Loading	TP Loading
1	MaxRate	N-Imperv	Roof wash off exponent	Roof wash off exponent
2	MinRate	MaxRate	Pavement wash off exponent	Pavement wash off exponent
3	Decay	N-perv	Green space wash off exponent	Roof maximum accumulation quantity
4	Dstore-Imperv	Decay	Removal rate by street sweeping	Roof wash off coefficient

3.3. Model Calibration and Validation

Model calibration and validation is based on the collected runoff samples for two storm events on 19–20 June 2018 and 9 April 2019. The total rainfall accumulation and duration for the June 2018 storm is 31.8 mm and 16 h, respectively. The April 2019 storm is a short-term intense rainfall event, with rainfall accumulation of 16.8 mm during a four-hour period. There are 5 and 11 dry days preceding 19–20 June 2018 and 9 April 2019, respectively. The June 2018 storm is used for model calibration, while the April 2019 storm is for model validation. We first calculated runoff over the four urban plots based on the runoff curve number (CN) method [56]. The CN values for residential, park, greenbelt, and commercial area are 92, 98, 80, and 95, respectively, according to the hydraulic properties of soil [56]. The TN and TP loadings are then computed by multiplying runoff with the concentrations of TN and TP (based on laboratorial analyses of collected runoff samples). The TN and TP loadings over the four sub-catchments are further compared against model simulation for model calibration and validation. For model calibration, we manually adjust the parameters (listed in Table 3) until the relative deviations between simulated and derived TP and TN loadings are within 30% [39]. The determined parameter sets are further used for the April 2019 storm for model validation, to test the applicability of the parameters for different storm events.

As can be seen from Table 4, there is a good match between simulated TN loading and the value derived from in-situ observations over the park plot during the June 2018 storm, with relative deviation less than 7%. The relative deviation between the simulated and derived TP loading is −11%. The simulation bias for TN loading over the residential plot is relatively large, but relative bias is still within 30%. The relative biases of TN loading are within 20% over the two urban plots during the model validation period (i.e., the April 2019 storm). However, the relative biases of the simulated TP loading are 33% on both two urban plots during the model validation, which is still within a reasonable range [57]. Relatively large biases in TP simulation might be associated with the small TP loadings over our study region.

Table 4. Relative deviation between simulated value and measured value.

Rainfall Event	Land Use Classes		TN	TP	Area (ha)
Calibration 19–20 June 2018	Residential area	Measured value (kg)	3.13	0.46	11.9
		Simulated value (kg)	4.08	0.39	
		Relative deviation (%)	30%	−15%	
	Park	Measured value (kg)	1.57	0.18	4.86
		Simulated value (kg)	1.68	0.16	
		Relative deviation (%)	7%	−11%	
Validation 9 April 2019	Greenbelt	Measured value (kg)	0.03	0.0009	3.53
		Simulated value (kg)	0.04	0.0006	
		Relative deviation (%)	20%	−33%	
	Commercial area	Measured value (kg)	0.32	0.02	0.78
		Simulated value (kg)	0.38	0.01	
		Relative deviation (%)	19%	−33%	

The simulated total runoff over the entire catchment is 738 mm. According to rain gauge observation, the total rainfall is 1195 mm over the entire period of 2018. This leads to a runoff ratio of 0.62. According to the national criteria of urban planning over China, runoff ratio is maintained within the range of 0.6–0.7 over urban regions with dense buildings. This indicates that our model can capture key feature of rainfall-runoff response over the catchment. In addition, the continuity error for surface runoff, flow rate, and water quality simulated by SWMM is less than 0.43%, 0.86%, and 0.51%, respectively. The model can reasonably capture the key features of storm runoff and pollutant loading over the study region and will be used for the following analysis.

4. Numerical Results and Discussion

4.1. Identification of Surface Non-Point Source Pollution Risk Areas

The simulated total TN and TP loadings over the entire study area is 8.08×10^4 kg and 0.66×10^4 kg, respectively. Figure 4 shows the pollution load averaged over contributing areas for each type of land use, i.e., total load divided by total area (with a unit of kg/ha). As we can see from Figure 4, the area-average loading of TN is significantly higher than TP over each land use/land cover type. More specifically, the averaged TN loading is the highest over residential land, followed by industrial land that contributes high TN loading per unit area. The same is true for TP loading.

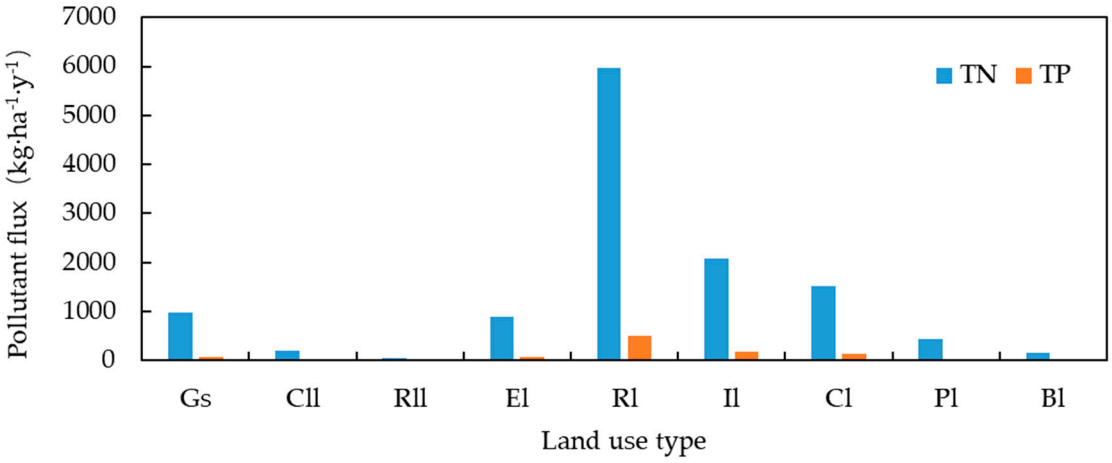

Figure 4. Pollutant flux of different land use types in 2018. The abbreviations on the x-axis are expanded as follows: Gs- Green spaces; Cll-Cultivated land; Rll-Religious land; El-Education land; Rl-Residential land; Il-Industrial land; Cl-Commercial land; Pl-Public services land; Bl-Bare land.

We further explore the factors that lead to the spatial variations of area-average loading of pollutants over different land use and land cover types. Previous studies show that pavement and roof are more impermeable than greenbelt, and their concentration of water quality index of runoff is generally higher than that of greenbelt [15,58]. The amounts of pollution from pavement and roof runoff are higher than that from greenbelt. Therefore, the higher area proportion of pavement and roof, the higher area-average loading of pollutants in land use type would be. However, we can see from Figure 3 that the proportion of pavement and roof on residential land is 77.4%, which is 7.4% lower than that on industrial land, even though residential land has a higher TN and TP pollution load. This is related to the cumulative loadings of pollutants on the surface. Previous studies show that residential land has higher cumulative pollutant loadings on the surface, about twice that over industrial land in our study area [48].

We classify area-averaged TN and TP loadings over the entire catchment into five grades based on the Natural Breaks (Jenks) method (see also Slocum [59] for details). The highest grade indicates the maximum area-averaged loading range of pollutants. Figure 5 shows the spatial distributions of the grading results for both TN and TP. The spatial distributions of TN and TP are overall consistent over the entire catchment, with the southeastern portion of the catchment showing the highest grade. Lower grades of TN and TP are mainly distributed over the southwestern portion of the catchment. The green area in the southwest of the study area is larger than that in the southeast. The total areas for each grade of TN and TP are also summarized (see the bar plots in Figure 5).

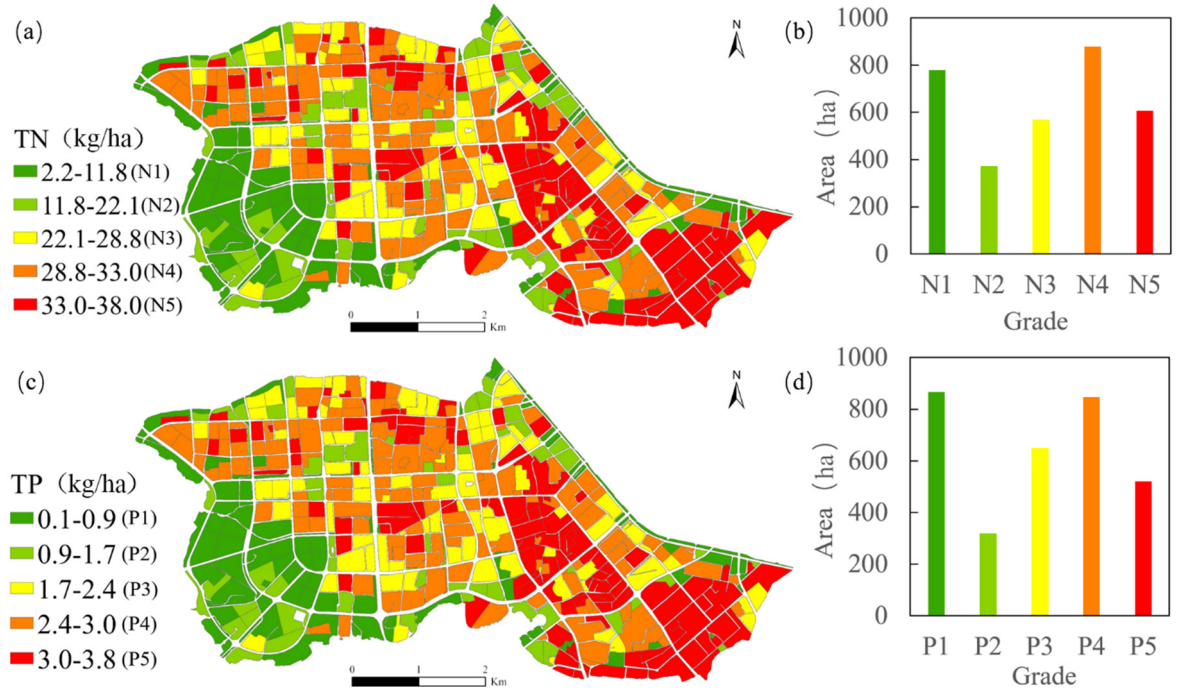

Figure 5. Spatial distribution of total nitrogen (TN) flux (**a**) and total phosphorus (TP) flux (**c**) in the study area and its area, (**b**,**d**) is the total areas corresponding to different TN and TP flux range values.

Figure 6 shows the sub-catchments with both highest grades of TN and TP. These sub-catchments are defined as the non-point source pollution risk areas. Therefore, the non-point source pollution risk area is determined based on pollutant flux (TN flux is greater than 33 kg/ha/year, TP flux is greater than 3 kg/ha/year). The identified spatial difference of pollution load is still consistent with the actual situation [7–10]. The area of non-point source pollution risk areas in the study area is 553.8 ha, mainly concentrated in the central east and southeast portion of the catchment. These regions are characterized with large residential and industrial land. Overall, the risk areas are mainly distributed over

six land use types, i.e., residential, industrial, commercial, education, public services, and religious land type. The total loadings of TN and TP of the six land use types are 3324 kg and 311 kg, respectively. The pollution load of each land use type is proportional to its area. The larger the land use type is, the larger the non-point source pollution load would be. Three land use/land cover types, i.e., residential land, industrial land, commercial land, account for 98% of the entire pollutant loading. Therefore, effective control measures of non-point source pollution need to particularly focus on these three land use types.

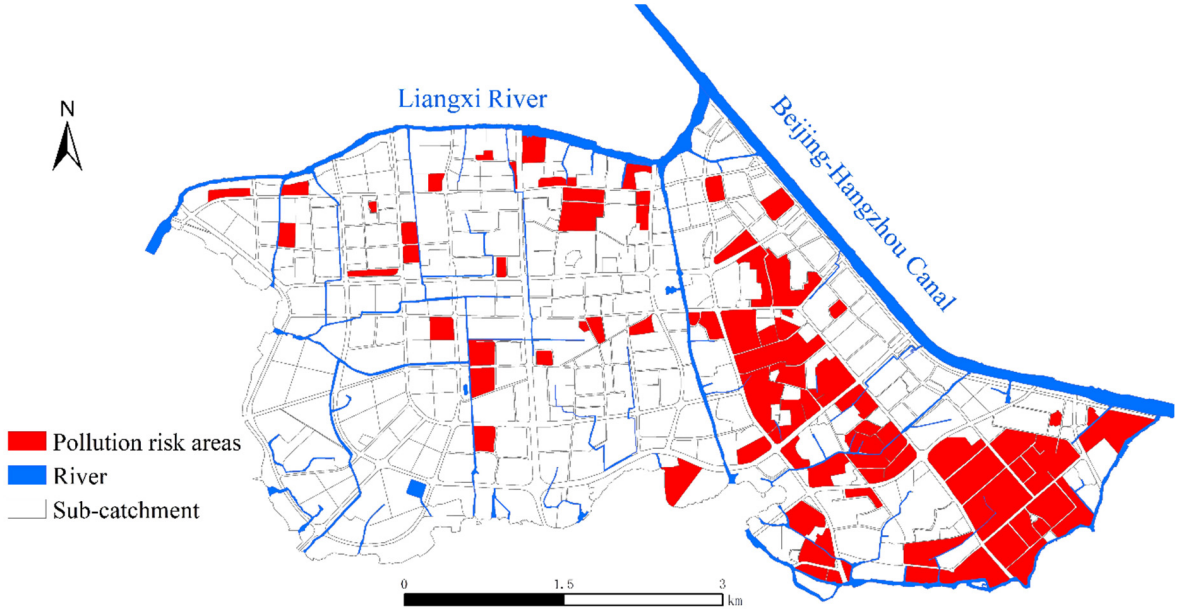

Figure 6. Surface non-point source pollution risk areas.

4.2. Correlation between Pollution Load and Time Influence Factors in the Risk Areas

The temporal variations of TN and TP are determined by the characteristics of rainfall, including rainfall accumulation, rainfall duration, rainfall intensity, and early drought days [21,22,60]. We examine the correlation between monthly surface non-point source pollution load in the risk areas and key properties of rainfall for all the rainfall events during 2018 (see Table 5 for results). There are 123 rainfall events during the year of 2018 in total. There is a significant positive correlation between rainfall accumulation and pollution load ($p < 0.01$) for both TN and TP. There is a significant positive correlation between rainfall duration, mean rainfall intensity, and pollution load ($p < 0.01$) for the months in January, May, June, and December. However, there is only significant positive correlation between the early drought days and TN pollution load in September ($p < 0.05$). Previous studies show the early drought days only plays a role in the non-point source pollution load during the initial stage of rainfall [61]. The insignificant correlations between early drought days and TN pollution load are possibly due to the simple treatment of background pollutant values and numerical modules in simulating the generation and accumulation processes of surface pollutants in the SWMM model [62].

Table 5. Correlation analysis of pollution load and its influencing factors.

Pollutant	Month	Rainfall	Rainfall Duration	Mean Rainfall Intensity	Early Drought Days
TN (TP)	January	0.99 ** (0.99 **)	0.87 ** (0.87 **)	0.79 ** (0.79 **)	0.05 (0.05)
	February	0.99 ** (0.95 **)	0.76 * (0.65)	0.67 (0.75)	0.28 (0.32)
	March	0.99 ** (0.99 **)	0.43 (0.43)	0.78 ** (0.78 **)	−0.01 (−0.01)
	April	0.99 ** (0.99 **)	0.89 ** (0.89 **)	0.79 ** (0.78 *)	0.20 (0.20)
	May	0.99 ** (0.98 **)	0.70 ** (0.69 **)	0.67 ** (0.69 **)	0.13 (0.13)
	June	0.99 ** (0.99 **)	0.94 ** (0.94 **)	0.82 ** (0.82 **)	0.36 (0.36)
	July	0.99 ** (0.98 **)	0.59 * (0.57 *)	0.89 ** (0.90 **)	0.01 (0.03)
	August	0.99 ** (0.99 **)	0.91 ** (0.87 **)	0.69 * (0.74 **)	−0.36 (−0.38)
	September	0.98 ** (0.98 **)	0.94 ** (0.94 **)	0.51 (0.75)	0.81 * (0.37)
	October	0.98 ** (0.98 **)	0.93 ** (0.93 **)	0.88 ** (0.88 *)	0.07 (0.07)
	November	0.98 ** (0.98 **)	0.79 * (0.79 *)	0.74 * (0.74 *)	−0.13 (−0.13)
	December	0.99 ** (0.99 **)	0.98 ** (0.98 **)	0.67 ** (0.67 **)	0.08 (0.08)

Note: the values in the table are Spearman's correlation coefficients; * is significant ($p < 0.05$) and ** is extremely significant ($p < 0.01$).

4.3. Sensitivity of Pollutant Loading to Different Source-Control Measures

'Source control' is the most direct and simple way of pollutant control, mainly for changing the surface permeability and surface sanitation. The control of "sink" and "end" stage involves the planning and control of municipal facilities construction, such as rainwater and sewage diversion system in urban drainage system, which is difficult for reconstruction and control of the highly urbanized areas. Therefore, we further evaluate the effectiveness of two source-control measures, i.e., increase the vegetation coverage and enhance road cleaning, in reducing TN and TP pollution loads over the pollution risk areas identified in Section 4.2.

4.3.1. Increase of Vegetation Coverage

Based on our field investigations, we found that vegetation coverage can be improved by changing the traditional building roofs to green roofs, changing the pavement in the park or courtyard to a permeable pavement, and building grass bio-retention swales or cells in the road boundary or the square. In this section, the reduction of non-point source pollution is realized by increasing the vegetation coverage over industrial, commercial, and residential land over the identified risk areas. According to the proportion of pavement, roof, and greenbelt and the proportion of non-point source pollution control set in previous studies [63,64], we increase the greenbelt coverage by 10% via reducing the coverage of pavement and roof by 5% each. If the pavement coverage in sub-catchment is small (less than 5%), the roof coverage will be reduced accordingly. In addition, the removal efficiency of BMPs pollutants in greenbelt was increased, which is equivalent to the function of low-impact development (LID) facilities. We set up four numerical scenarios of 5%, 10%, 15%, and 20% BMPs pollutant removal efficiencies. The total pollutant loadings for the four scenarios are compared against the default simulation as mentioned in Section 3. The results are compared over three different seasons, i.e., the dry season (December–January–February), the normal season (March–April, October–November), and the wet season (May–September).

As can be seen from Figure 7, the largest reduction of pollutant loading is observed during the wet season. This is most likely associated with high rainfall in wet season than that in normal season in 2018. Previous studies show that heavy rainfalls have a greater capacity for pollutant mobilization and infiltration [61]. Especially when pollutants accumulate for a long time on sunny days, heavy rainfall will generate a large amount of pollution load, and the reduction effect of pollution control measures will be more obvious. The annual pollution reduction of TN is 1163 kg, 2744 kg, 4217 kg, and 5748 kg, respectively, and the annual pollution reduction of TP was 113 kg, 212 kg, 169 kg, and

169 kg, respectively, for the four BMPs pollutant removal efficiencies. The higher the pollutant removal efficiency is, the greater the pollution reduction amount of TN would be. The annual pollution reduction of TP is significantly increased with increasing BMPs pollutant removal efficiency, from the BMPs pollutant removal efficiency at 0 to 10%. However, from the BMPs pollutant removal efficiency of 10% to 20%, the reduction effect for TP pollution load remain unchanged. Our result is consistent with Baek et al. [65] showing that the total pollutant load is the largest when the LID coverage is 20%.

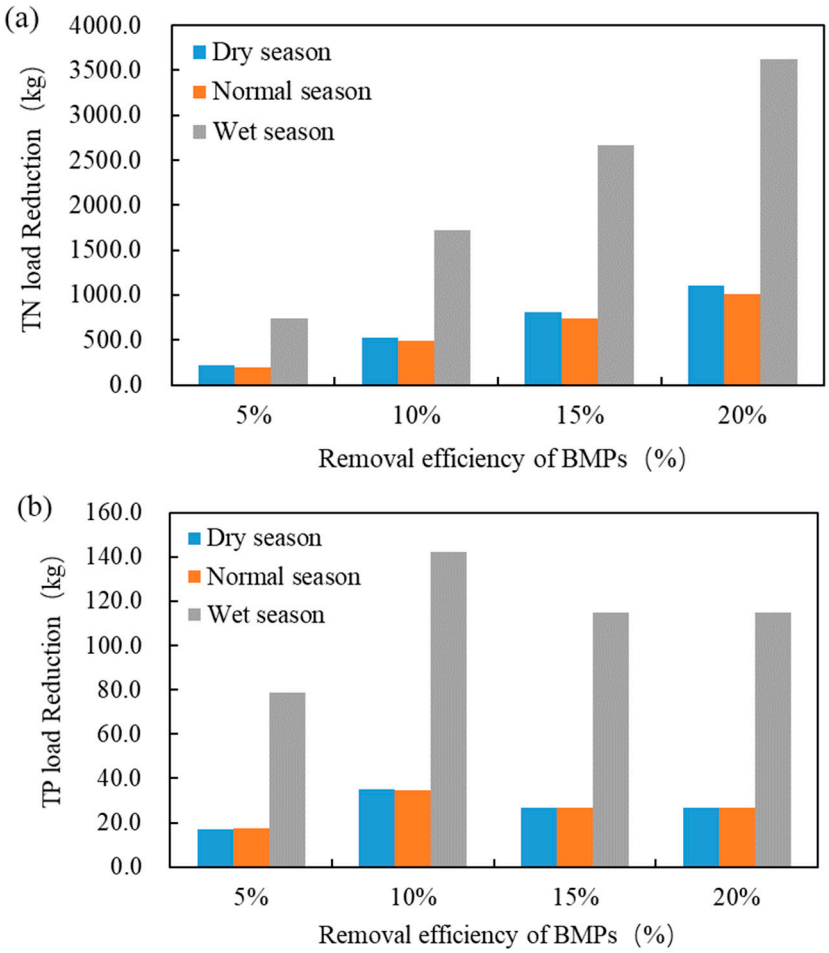

Figure 7. TN (**a**) and TP (**b**) reduction at different removal efficiency of best management practices (BMPs).

4.3.2. Enhanced the Road Cleaning

Three numerical scenarios of road cleaning are set up in our study. For the first cleaning situation, the frequency of road cleaning is three times a day, the cleaning efficiency is 70%; for the second cleaning situation, the frequency of road cleaning is twice a day, the cleaning efficiency is 80%; for the third cleaning situation, the frequency of road cleaning is three times a day, the cleaning efficiency is 80%. In the default model simulation, the road cleaning frequency is twice a day, and the cleaning frequency is 70%. The total pollutant loadings for the three scenarios are compared against the default simulation as mentioned in Section 3.

As we can see from Figure 8, the higher the frequency and efficiency of road cleaning is, the greater the amount of pollutant reduction would be. The pollution reduction rate is the smallest in the dry season and the largest in the wet season. The annual pollution reduction of TN pollutants is 146 kg, 78 kg, and 201 kg, respectively, and the annual pollution reduction of TP pollutants was 9.5 kg, 4.8 kg, and 13 kg, respectively, for the three

situations. These reduction rates are much smaller than those shown in the scenarios with increased green coverages (Figure 7).

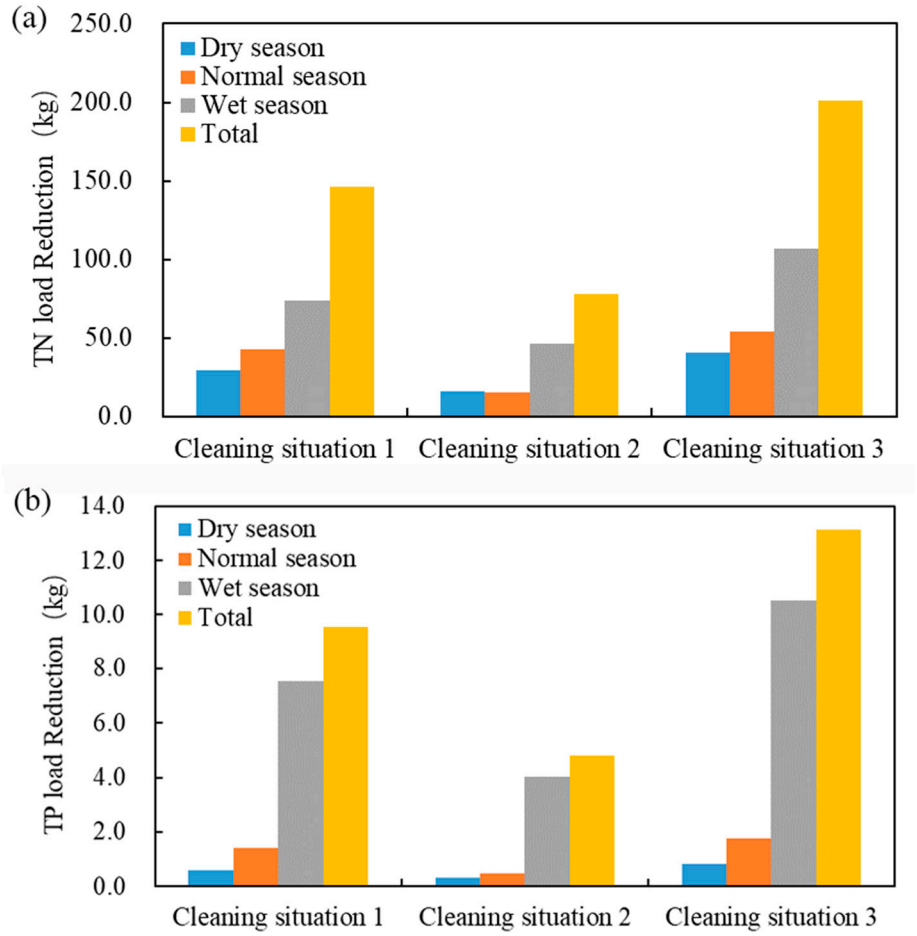

Figure 8. TN (**a**) and TP (**b**) reduction at different frequency and efficiency of road cleaning. Cleaning situation 1: The frequency of road cleaning is three times a day, the cleaning efficiency is 70%; Cleaning situation 2: The frequency of road cleaning is twice a day, the cleaning efficiency is 80%; Cleaning situation 3: The frequency of road cleaning is three times a day, the cleaning efficiency is 80%.

From the TN and TP pollution reduction, the pollution reduction in cleaning situation 3 is greater than that in cleaning situation 1. The pollution reduction in cleaning situation 1 is greater than that in cleaning situation 2 (Figure 8). The results indicated that it is more effective to improve the cleaning frequency than the cleaning efficiency to reduce the urban non-point source pollutants.

5. Summary and Conclusions

In this study, we examine the non-point source pollutant loading over an urban catchment based on the SWMM model and in-situ samplings. Two measured rainfall events were used to calibrate and validate the model. We identify the spatial and temporal distributions of surface non-point source pollution based on the numerical experiments, and further test the effectiveness of different source-control measures in the reduction of urban non-point source pollution. The main conclusions are as follows.

The highest loadings of both TN and TP are mainly distributed over residential and industrial land use types in the eastern part of the study area. This is mainly due to high areal proportions of pavement and roofs over these land use types as well as accumulative loadings over these land surfaces units. There are six land use types in the surface non-

point source pollution risk areas (i.e., high TP and TN loadings), among which pollution load over three land use types, residential, industrial, and commercial land, account for 98% of the total load.

Temporal variations for both TN and TP loadings are consistent, with abrupt changes mainly during late summer and early autumn. Rainfall accumulation of each rainfall event in the year is the main factor affecting the temporal variations of pollution load. Rainfall duration and mean rainfall intensity also influence on the non-point source pollution. There is almost no correlation between early drought days and pollution load for TN and TP.

Numerical simulations show that it is more effective to increase the urban vegetation coverage rate than to enhance the road cleaning. Under the condition of enhanced road cleaning, it is more effective to improve the frequency of road cleaning than the efficiency of road cleaning. Due to data limitations, we only investigate the effectiveness of source-control measures. Additional pollutant-control measures, such as rain barrel, bio-retention cell, and infiltration trench, can be investigated in future studies.

One caveat of the present study is the results are predominately based on numerical simulations, even though the model has been carefully calibrated against in-situ samplings. Additional rainfall events and storm runoff samples are needed to further increase the credibility of the model. Long-term monitoring or intense field surveys can be a good compliment to numerical studies but can be expensive and labor-intensive. For instance, Salerno et al. [66] used float switches connected to a continuous recording device to conduct two years of combined sewer overflows monitoring, and successfully monitored 252 events. However, it should be noted that the float switches need to be cleaned up once every two weeks which is labor-intensive. Effective monitoring networks are limited worldwide [67]. Therefore, we believe the numerical simulations presented in this study provides the first step to better understand the spatial and temporal characteristics of pollutant loadings (such as TN and TP) over complex urban environments, and serve the basis for the establishment of long-term monitoring network. We also note that the SWMM model to some extent simplifies the generation and accumulation process of non-point pollutants. There are some studies that demonstrate efforts to the modeling framework. For instance, Wang, et al. [68] applied the model they developed by considering residual pollutant after the storm event to an urban catchment in Los Angeles County, U.S., and found that the developed model is more capable of simulating non-point source pollution. Future studies need to incorporate state-of-art modeling tools, together with the utility of intense in-situ samplings, to improve our knowledge on the dynamics of non-point source pollutants in complex urban environments.

Author Contributions: Conceptualization, Y.P., J.G. and L.W.; data curation, J.G., Q.Y. and Z.R.; funding acquisition, L.W.; investigation, J.G., Q.Y. and Z.R.; methodology, Y.P.; project administration, L.W.; resources, L.W.; software, L.Y.; validation, Y.P. and L.Y.; writing—original draft, Y.P.; writing—review & editing, Y.P., J.G. and L.Y. All authors have read and agreed to the published version of the manuscript.

Funding: This research was funded by the Strategic Priority Research Program of the Chinese Academy of Science (XDA230402), the Major Science and Technology Program for Water Pollution Control and Treatment (2017ZX07203002-02-01) and the Nanjing Water Science and Technology Project (201806).

Institutional Review Board Statement: Not applicable.

Informed Consent Statement: Not applicable.

Data Availability Statement: The data presented in this study are available on request from the corresponding author. The data are not publicly available due to privacy.

Acknowledgments: The authors would like to acknowledge Zhuoyang Yao for his assistance in filed studies as well as Xi Wang and Chunhua Hu for laboratory analysis.

Conflicts of Interest: The authors declare that they have no conflict of interest.

References

1. Shao, M.; Zhao, G.; Kao, S.-C.; Cuo, L.; Rankin, C.; Gao, H. Quantifying the effects of urbanization on floods in a changing environment to promote water security—A case study of two adjacent basins in Texas. *J. Hydrol.* **2020**, *589*, 125154. [CrossRef]
2. Qi, M.; Yang, Y.; Zhang, X.; Zhang, X.; Wang, M.; Zhang, W.; Lu, X.; Tong, Y. Pollution reduction and operating cost analysis of municipal wastewater treatment in China and implication for future wastewater management. *J. Clean. Prod.* **2020**, *253*, 120003. [CrossRef]
3. Müller, A.; Österlund, H.; Marsalek, J.; Viklander, M. The pollution conveyed by urban runoff: A review of sources. *Sci. Total Environ.* **2020**, *709*, 136125. [CrossRef] [PubMed]
4. Shen, Z.; Zhong, Y.; Huang, Q.; Chen, L. Identifying non-point source priority management areas in watersheds with multiple functional zones. *Water Res.* **2015**, *68*, 563–571. [CrossRef] [PubMed]
5. Robb, G.A.; Novotny, V.; Olem, H. Water Quality: Prevention, Identification and Management of Diffuse Pollution. *Geogr. J.* **1996**, *162*, 109. [CrossRef]
6. Novotny, V. Integrating Diffuseinonpoint Pollution Control and Water Body Restoration into Watershed Management. *J. Am. Water Resour. Assoc.* **1999**, *35*, 717–727. [CrossRef]
7. Yu, D.; Li, J.; Zhang, Y.; Wang, H.; Guo, B.; Zheng, L. Enantioseletive bioaccumulation of tebuconazole in earthworm Eisenia fetida. *J. Environ. Sci.* **2012**, *24*, 2198–2204. [CrossRef]
8. Pitt, R.; Field, R.; Lalor, M.; Brown, M. Urban stormwater toxic pollutants: Assessment, sources, and treatability. *Water Environ. Res.* **1995**, *67*, 260–275. [CrossRef]
9. Sundt, P.; Schulze, P.; Syversen, F. *Sources of Microplastic-Pollution to the Marine Environment*; Report no: M-321 | 2015; Mepex for the Norwegian Environment Agency: Trondheim, Norway, 2014.
10. Bressy, A.; Gromaire, M.-C.; Lorgeoux, C.; Chebbo, G. Alkylphenols in atmospheric depositions and urban runoff. *Water Sci. Technol.* **2011**, *63*, 671–679. [CrossRef]
11. Wang, J.; Luo, B.; Chen, M.; Xie, S.; Tang, G.; Li, N.; Wu, H.; Luo, X. Study on the characteristics of urban non-point source pollution and its discharge load: A case study for Neijiang, Sichuan province. *Ecol. Environ. Sci.* **2014**, *23*, 151–156.
12. Liu, L.; Dong, Y.; Kong, M.; Zhou, J.; Zhao, H.; Tang, Z.; Zhang, M.; Wang, Z.-P. Insights into the long-term pollution trends and sources contributions in Lake Taihu, China using multi-statistic analyses models. *Chemosphere* **2020**, *242*, 125272. [CrossRef] [PubMed]
13. Hobbiea, S.E.; Finlaya, J.C.; Jankea, B.D.; Nidzgorskia, D.A.; Milletb, D.B.; Bakerc, L.A. Contrasting nitrogen and phosphorus budgets in urban watersheds and implications for managing urban water pollution. *Proc. Natl. Acad. Sci. USA* **2017**, *114*, E4116. [CrossRef] [PubMed]
14. Liu, Y.; Chen, W.; Li, D.; Huang, Z.; Shen, Y.; Liu, Y. Cyanobacteria-/cyanotoxin-contaminations and eutrophication status before Wuxi Drinking Water Crisis in Lake Taihu, China. *J. Environ. Sci.* **2011**, *23*, 575–581. [CrossRef]
15. Luo, B.; Li, N.; Wang, J. Review of Urban Nonpoint Pollution Formation and Characteristics. *Sichuan Environ.* **2012**, *31*, 110–113. [CrossRef]
16. Yao, L.; Li, J.; Wei, W. Exploring the Linkage between Urban Flood Risk and Spatial Patterns in Small Urbanized Catchments of Beijing, China. *Int. J. Environ. Res. Public Health* **2017**, *14*, 239. [CrossRef] [PubMed]
17. Zhang, L.; Lu, W.; Hou, G.; Gao, H.; Liu, H.; Zheng, Y. Coupled analysis on land use, landscape pattern and nonpoint source pollution loads in Shitoukoumen Reservoir watershed, China. *Sustain. Cities Soc.* **2019**, *51*, 51. [CrossRef]
18. Hood, M.J.; Clausen, J.C.; Warner, G.S. Comparison of Stormwater Lag Times for Low Impact and Traditional Residential Development. *J. Am. Water Resour. Assoc.* **2007**, *43*, 1036–1046. [CrossRef]
19. Meierdiercks, K.L.; Smith, J.A.; Baeck, M.L.; Miller, A.J. Analyses of Urban Drainage Network Structure and its Impact on Hydrologic Response1. *J. Am. Water Resour. Assoc.* **2010**, *46*, 932–943. [CrossRef]
20. Cheng, H.; Lin, C.; Wang, L.-J.; Lin, C.; Peng, L.; Zhu, C. The Influence of Different Forest Characteristics on Non-point Source Pollution: A Case Study at Chaohu Basin, China. *Int. J. Environ. Res. Public Health* **2020**, *17*, 1790. [CrossRef]
21. Zhang, L.; Zhao, B.; Xu, G.; Guan, Y. Characterizing fluvial heavy metal pollutions under different rainfall conditions: Implication for aquatic environment protection. *Sci. Total Environ.* **2018**, *635*, 1495–1506. [CrossRef]
22. Li, L.-Q.; Yin, C.; Kong, L.-L.; He, Q.-C. Effect of antecedent dry weather period on urban storm runoff pollution load. *Environ. Sci.* **2007**, *28*, 2287–2293.
23. Lian, Q.; Yao, L.; Ahmad, Z.U.; Lei, X.; Islam, F.; Zappi, M.E.; Gang, D.D. Nonpoint source pollution. *Water Environ. Res.* **2019**, *91*, 1114–1128. [CrossRef] [PubMed]
24. Kim, S.-W.; Park, J.-S.; Kim, D.; Oh, J.M. Runoff characteristics of non-point pollutants caused by different land uses and a spatial overlay analysis with spatial distribution of industrial cluster: A case study of the Lake Sihwa watershed. *Environ. Earth Sci.* **2013**, *71*, 483–496. [CrossRef]
25. Jung, J.-W.; Park, H.-N.; Yoon, K.-S.; Choi, D.-H.; Lim, B.-J. Event mean concentrations (EMCs) and first flush characteristics of runoff from a public park in Korea. *J. Korean Soc. Appl. Biol. Chem.* **2013**, *56*, 597–604. [CrossRef]
26. USEPA. Hydrological Simulation Program—FORTRAN (HSPF). Available online: https://www.epa.gov/ceam/hydrological-simulation-program-fortran-hspf#Application (accessed on 20 July 2020).
27. USEPA. Storm Water Management Model (SWMM). Available online: https://www.epa.gov/water-research/storm-water-management-model-swmm (accessed on 5 February 2020).

28. Lundgren, J. Mathematical models and computer programs [STORM, storage treatment overflow runoff model] in storm water treatment. *Vatten* **1977**. Available online: https://agris.fao.org/agris-search/search.do?recordID=SE19780264293 (accessed on 10 January 2020). (In Sweedish).
29. Alley, W.M.; Smith, P.E. *Distributed Routing Rainfall-Runoff Model-Version II*; Open-File Report 1978; U.S. Geological Survey: Reston, VA, USA, 1982; p. 201.
30. McPherson, T.; Burian, S.; Turin, H.; Stenstrom, M.; Suffet, I. Comparison of the pollutant loads in dry and wet weather runoff in a southern California urban watershed. *Water Sci. Technol.* **2002**, *45*, 255–261. [CrossRef] [PubMed]
31. Yuan, Y.; Hall, K.; Oldham, C. A preliminary model for predicting heavy metal contaminant loading from an urban catchment. *Sci. Total Environ.* **2001**, *266*, 299–307. [CrossRef]
32. Alvarez, S.; Asci, S.; Vorotnikova, E. Valuing the Potential Benefits of Water Quality Improvements in Watersheds Affected by Non-Point Source Pollution. *Water* **2016**, *8*, 112. [CrossRef]
33. He, C.; Zhang, L.; Demarchi, C.; Croley, T.E. Estimating point and non-point source nutrient loads in the Saginaw Bay watersheds. *J. Great Lakes Res.* **2014**, *40*, 11–17. [CrossRef]
34. Fonseca, A.R.; Botelho, C.; Boaventura, R.A.; Vilar, V.J. Integrated hydrological and water quality model for river management: A case study on Lena River. *Sci. Total. Environ.* **2014**, 474–489. [CrossRef]
35. Reginato, M.; Piechota, T. Nutrient Contribution of Nonpoint Source Runoff in the Las Vegas Valley. *J. Am. Water Resour. Assoc.* **2004**, *40*, 1537–1551. [CrossRef]
36. Leite, M.E.; Koide, S. Monitoring and Modeling of the Urban Water Drainage Basin of Lake Paranoá. In Proceedings of the 13th IWA/IAHR International Conference on Urban Drainage (ICUD 2014), Sarawak, Malaysia, 7–11 September 2014.
37. Tsihrintzis, V.A.; Hamid, R. Runoff quality prediction from small urban catchments using SWMM. *Hydrol. Process.* **1998**, *12*, 311–329. [CrossRef]
38. Pan, Y. Study on Capability of the Initial Rainwater Detention Tanks in Separate System Based on SWMM. Master's Thesis, Chongqing University, Chongqing, China, May 2015.
39. Zhao, L.; Yang, F.L.; Yuan, G.L.; Wang, J.S.; Zhu, Y.G. Simulation of the quantity and quality of the urban runoff. *Acta Ecol. Sin.* **2015**, *35*, 1961–1972.
40. Yan, L.; Xiong, L.; Wang, J. Analysis of Storm Runoff Simulation in Typical Urban Region of Wuhan Based on SWMM. *J. Water Resour. Res.* **2014**, *3*, 216–228. [CrossRef]
41. Cong, X.-Y.; Ni, G.-H.; Hui, S.-B.; Tian, F.-Q.; Zhang, T. Smiulative analysis on storm flood in typical urban region of Beijing based on SWMM. *Water Resour. Hydropower Eng.* **2006**, *37*, 64–67.
42. Endreny, T.; Wood, E.F. Watershed Weighting of Export Coefficients to Map Critical Phosphorous Loading Areas. *J. Am. Water Resour. Assoc.* **2003**, *39*, 165–181. [CrossRef]
43. Chen, Y.; Zhang, Z.; Yang, C.; Wan, L.; Ye, C.; Zhang, J.; Li, Q. Identifying risk areas and risk paths of non-point source pollution in Wuhua River Basin. *Acta Geogr. Sin.* **2018**, *73*, 1765–1777. [CrossRef]
44. Luan, B.; Yin, R.X.; Xu, P.; Wang, X.; Yang, X.M.; Zhang, L.; Tang, X.Y. Evaluating Green Stormwater Infrastructure strategies efficiencies in a rapidly urbanizing catchment using SWMM-based TOPSIS. *J. Clean. Prod.* **2019**, *223*, 680–691. [CrossRef]
45. Yang, G.; Bowling, L.C.; Cherkauer, K.A.; Pijanowski, B.C.; Niyogi, D. Hydroclimatic Response of Watersheds to Urban Intensity: An Observational and Modeling-Based Analysis for the White River Basin, Indiana. *J. Hydrometeorol.* **2010**, *11*, 122–138. [CrossRef]
46. Huishu, L.; Lei, Q.; Xinyu, Z.; Haw, Y.; Hongyuan, W.; Limei, Z.; Liu, H.; Huang, J.-C.; Tianzhi, R.; Jiaogen, Z.; et al. Effects of anthropogenic activities on long-term changes of nitrogen budget in a plain river network region: A case study in the Taihu Basin. *Sci. Total Environ.* **2018**, *645*, 1212–1220. [CrossRef]
47. Nobre, R.L.G.; Caliman, A.; Cabral, C.R.; Araújo, F.D.C.; Guérin, J.; Dantas, F.D.C.C.; Quesado, L.B.; Venticinque, E.M.; Guariento, R.D.; Amado, A.M.; et al. Precipitation, landscape properties and land use interactively affect water quality of tropical freshwaters. *Sci. Total Environ.* **2020**, *716*, 137044. [CrossRef]
48. Guo, J.; Pan, Y.; Zuo, P.; Xu, Y.; Wang, Q.; Ma, J.; Wang, L. Accumulation and wash-off characteristics of surface pollutant and identification of risk areas on urban land uses in a lakeside city, Wuxi, China. *Urban Water J.* **2019**, *16*, 323–333. [CrossRef]
49. James, W.; Rossman, L.A.; James, W.R. *User's Guide to SWMM5*; CHI: Guelph, ON, Canada, 2010.
50. Rossman, L.A. *Storm Water Management Model User's Manual, Version 5.0*; National Risk Management Research Laboratory, Office of Research and Development, US Environmental Protection Agency: Washington, DC, USA, 2010.
51. Palla, A.; Gnecco, I. Hydrologic modeling of Low Impact Development systems at the urban catchment scale. *J. Hydrol.* **2015**, *528*, 361–368. [CrossRef]
52. Yazdi, M.N.; Ketabchy, M.; Sample, D.J.; Scott, D.; Liao, H. An evaluation of HSPF and SWMM for simulating streamflow regimes in an urban watershed. *Environ. Model. Softw.* **2019**, *118*, 211–225. [CrossRef]
53. McCuen, R.H.; Johnson, P.A.; Ragan, R.M. *Highway Hydrology, Hydraulic Design Series No. 2*; Federal Highway Administration: Washington, DC, USA, 1996.
54. American Society of Civil Engineers and Water Environment Federation. *Design and Construction of Urban Stormwater Management Systems*; American Society of Civil Engineers and Water Environment Federation: Reston, VA, USA, 1992.
55. Tan, M.; Yao, J.; Zhang, Z.; Pu, P.; Wei, T. Analysis and application of sensitivity of water quality parameter based on SWMM of Morris. *J. Water Resour. Water Eng.* **2015**, *26*, 117–122. [CrossRef]

56. Soil Conservation Service, U.S. *Department of Agriculture. Urban Hydrology for Small Watersheds*; Engineering Division, Soil Conservation Service, U.S. Department of Agriculture: Washington, DC, USA, 1975; Volume 55, p. 81.
57. Li, C.; Zheng, X.; Zhao, F.; Wang, X.; Cai, Y.; Zhang, N. Effects of Urban Non-Point Source Pollution from Baoding City on Baiyangdian Lake, China. *Water* **2017**, *9*, 249. [CrossRef]
58. Ou, Y.; Rousseau, A.N.; Yan, B.; Wang, L.; Zhang, Y. Grass barriers for mitigating diffuse pollution within a source water area—A case study of Northeast China. *Agric. Water Manag.* **2021**, *243*, 106461. [CrossRef]
59. Slocum, T.A. *Thematic Cartography and Geovisualization*; Pearson Prentice Hall: Upper Saddle River, NJ, USA, 2009.
60. Zhao, J.Q. *Urban Surface Runoff Pollution and Control*; China Environmental Science Press: Beijing, China, 2002.
61. Hernández-Crespo, C.; Fernández-Gonzalvo, M.; Martín, M.; Andrés-Doménech, I. Influence of rainfall intensity and pollution build-up levels on water quality and quantity response of permeable pavements. *Sci. Total Environ.* **2019**, *684*, 303–313. [CrossRef]
62. Dotto, C.B.S.; Kleidorfer, M.; Deletic, A.; Rauch, W.; McCarthy, D.; Fletcher, T. Performance and sensitivity analysis of stormwater models using a Bayesian approach and long-term high resolution data. *Environ. Model. Softw.* **2011**, *26*, 1225–1239. [CrossRef]
63. Ma, M.; Li, J.; Deng, C. Analysis of urban waterlogging and pollution load based on SWMM model. *J. Hydroelectr. Eng.* **2017**, *36*, 62–72. [CrossRef]
64. Xue, T.Y.; Xu, L.Z.; Li, C.M.; Cheng, G. Simulated analysis of water quality effect of bioremediation pond water. *Water Resour. Hydropower Eng.* **2008**, *49*, 121–127.
65. Baek, S.-S.; Ligaray, M.; Pyo, J.; Park, J.-P.; Kang, J.-H.; Pachepsky, Y.; Chun, J.A.; Cho, K.H. A novel water quality module of the SWMM model for assessing low impact development (LID) in urban watersheds. *J. Hydrol.* **2020**, *586*, 124886. [CrossRef]
66. Salerno, F.; Gaetano, V.; Gianni, T. Urbanization and climate change impacts on surface water quality: Enhancing the resilience by reducing impervious surfaces. *Water Res.* **2018**, *144*, 491–502. [CrossRef] [PubMed]
67. Bell, C.D.; Tague, C.; McMillan, S. Modeling Runoff and Nitrogen Loads from a Watershed at Different Levels of Impervious Surface Coverage and Connectivity to Storm Water Control Measures. *Water Resour. Res.* **2019**, *55*, 2690–2707. [CrossRef]
68. Wang, L.; Wei, J.; Huang, Y.; Wang, G.; Maqsood, I. Urban nonpoint source pollution buildup and washoff models for simulating storm runoff quality in the Los Angeles County. *Environ. Pollut.* **2011**, *159*, 1932–1940. [CrossRef]